Digital Object Identifier 10.1109/TPEL.2018.2840961

IEEE Transactions on Power Electronics

A New Voltage Balancing Technique for a Three-Stage Modular Smart Transformer Interfacing a DC Multibus

Santa Pugliese
Markus Andresen
Rosa A. Mastromauro
Giampaolo Buticchi
Silvio Stasi
Marco Liserre

Suggested Citation

S. Pugliese, M. Andresen, R. A. Mastromauro, G. Buticchi, S. Stasi and M. Liserre, "A New Voltage Balancing Technique for a Three-Stage Modular Smart Transformer Interfacing a DC Multibus," in IEEE Transactions on Power Electronics, vol. 34, no. 3, pp. 2829-2840, March 2019

A New Voltage Balancing Technique for a Three-Stage Modular Smart Transformer Interfacing a DC Multibus

Sante Pugliese, *Member, IEEE*, Markus Andresen, *Member, IEEE*, Rosa A. Mastromauro, *Member, IEEE*, Giampaolo Buticchi, *Senior Member, IEEE*, Silvio Stasi, and Marco Liserre , *Fellow, IEEE*

***Abstract*—DC smart grids represent an alternative to traditional ac power distribution systems. The power conversion stage, interfacing the ac and the dc distribution systems, is the enabling technology to manage multiple dc loads and sources. The three-stage smart transformer (ST) is a promising solution, because it includes a dc–dc power conversion stage providing a dc multibus in output. The modular ST architecture supplies several dc outputs, which allow interfacing a dc smart grid with the ac power system. In this paper, the three-stage ST is based on a cascaded H-bridge (CHB) converter for the ac–dc power conversion, whereas dual active bridge (DAB) converters are adopted for the dc–dc power conversion stage. The peculiarity is that the dc voltage balancing is performed by the dc–dc power conversion stage instead of the CHB converter. It is advantageous for dc smart grids applications where the power sharing among the dc sources and loads is often not balanced. The design of the entire control system is based on the detailed small signal model of the ac–dc and dc–dc power conversion stages of the ST. High dynamic performance of the voltage balancing is fulfilled due to the commonly high switching frequency of the DAB converters.**

***Index Terms*—Cascaded H-bridge (CHB) converter, dc smart grids, dc voltage control, dual active bridge (DAB) converter, smart transformer (ST).**

This work was supported in part by the European Union/Interreg V-A Germany-Denmark, under PE: Region Project, in part by the European Research Council under the European Union's Seventh Framework Programme (FP/2007-2013)/ERC Grant Agreement no. 616344—HEART, in part by the Ningbo Science and Technology Beauro under Grant 2013A31012, and in part by the National Natural Science Foundation under Grant 51650110507.

S. Pugliese, M. Andresen and M. Liserre are with the Chair of Power Electronics, Christian-Albrechts Universit...at zu Kiel, Kiel 24143, Germany (e-mail: sapu@tf.uni-kiel.de; ma@tf.uni-kiel.de; buticchi@ieee.org; liserre@ieee.org).

R. A. Mastromauro is with the Department of Information Engineering, University of Florence, Florence 50139, Italy (e-mail: rosaanna. mastromauro@unifi.it).

G. Buticchi is with the Faculty of Science and Engineering, University of Nottingham Ningbo China, Ningbo 315100, China (email: Giampaolo. Buticchi@nottingham.edu.cn).

S. Stasi is with the Department of Electrical and Information Engineering, Politecnico di Bari, Bari 70125, Italy (e-mail: sante.pugliese@poliba.it; silvio.stasi@poliba.it).

I. Introduction

DC POWER distribution systems have gained interest in the last years both in transportation applications and in smart grids due to the possibility to increase the efficiency of the system, reducing the number of power conversion stages, and avoiding harmonic distortion and reactive power management issues [1]–[6]. Nevertheless, one of the main obstacles toward the spread of the dc smart grids is represented by the difficulty to manage multiple dc connections, interfacing with the main ac power distribution system, and ensuring flexible operation. DC smart grids supply the loads autonomously in island operation, or the same loads could be supplied by an active rectifier (ac–dc) connected to the ac power distribution system. The storage systems inside the dc smart grid should be charged directly by the dc sources or by the ac power system through the active rectifier [7]. Hence, the role of the ac–dc power conversion stage is pivotal.

Looking at the future development of the ac power distribution system, a lot of recent research has been devoted to the power electronics interface, which enables to replace the traditional transformer with a smart transformer (ST) [8]–[13]. The aim of the ST is to provide multiple and flexible connections and to provide advanced control functionalities, which the conventional transformer was not able to provide. It has been demonstrated that modular STs can provide higher reliability and availability than nonmodular topologies due to fault tolerance capability and possible reconfiguration in case of faults [14]–[16].

Among the possible ST topologies, the three-stage ST is based on a first ac–dc power conversion stage connected to the MV distribution system, a second dc–dc power conversion stage, which fulfills galvanic isolation and voltage gain variation, and a last dc–ac power conversion stage for providing the LV output [17], [18]. In case of modular topologies, the dc–dc power conversion stage provides multiple and flexible outputs, which can be combined in order to create a dc multibus [4], [19]. Hence, in this scenario, the first two stages of a three-stage modular ST can represent the enabling technology to interface the dc smart grids with the main ac power system.

Analyzing the power converters topologies, the cascaded H-bridge (CHB) converter, which consists of several H-bridges connected in series for each phase, is recognized as a

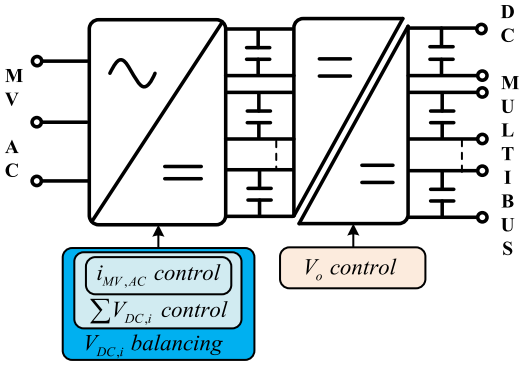

Fig. 1. Control structure of the first and the second stage of a three-stage ST where the ac–dc stage is in charge of the dc voltage balancing function.

potential candidate for the ST, because of its modularity, scalability, and high power quality performance. Focusing on the CHB converter, the dc voltage balancing among the different power cells has represented one of the main research topics in order to avoid overvoltages on the power devices. Numerous dc voltage balance techniques have been developed [20]–[26]. These techniques have been applied to the ST too, where commonly the ac–dc power conversion stage is in charge of the dc voltage balancing. In particular in [27]–[29], a review of the CHB dc voltage balancing techniques for ST application is presented. Many of these techniques aim to achieve both voltage and power balance [30], [31]. Differently, for dc smart grids applications, the modular ST has to guarantee the possibility to operate with power unbalances among the different power conversion cells and maintaining the dc-links voltages balanced. Indeed, considering the dc smart grids operation, storages, loads, and sources cannot be assumed processing the same power at each dc link. Instead, the loads are supplied to maintain the reference dc voltage value. Besides, recent research in the ST control, such as the power routing technique [32], [33], suggests also to manage different powers by the different power conversion cells in order to increase the ST reliability.

In Fig. 1, the first two stages of a three-stage ST are shown where the ac–dc power conversion stage is in charge of the dc voltage balancing. Each power cell of the CHB converter is connected to a dual active bridge (DAB) converter, as shown in Fig. 2, creating a dc multibus. The DAB converter topology offers many advantages, such as bidirectional power flow, high step up/down capabilities, and zero voltage switching, depending on the operating condition. The bidirectional power flow capability makes it an attractive choice when it is needed to control power exchange between energy storage and loads, enabling power flow in both directions. The high step up/down voltage capability provides flexibility to the dc multibus thanks to the possibility to extend the voltage range and to ensure galvanic isolation avoiding faults propagation. In Figs. 1 and 2, $V_{\mathrm{dc},i}$ denotes the ith output voltage of the CHB converter and V_o denotes the output voltage of the DAB converters. The dc links provided in output by the DAB converters can be connected to loads, storage, and dc sources separately or can be connected in parallel on the basis of the dc smart grid configuration.

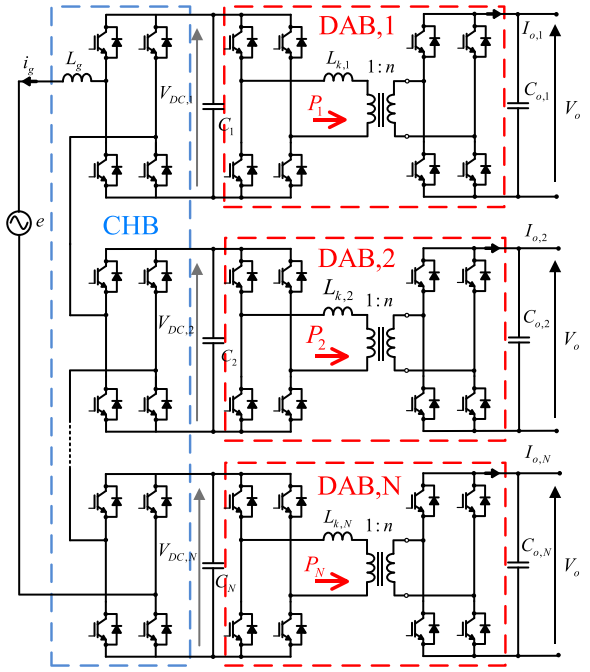

Fig. 2. First and second stage of a three-stage modular ST based on CHB and DAB converters.

Since loads are commonly not equal, the possibility to balance the dc voltages in the dc–dc power conversion stage instead of the first stage (CHB converter) results advantageous due to the proximity to the dc smart grid distribution system. It represents the main goal of the present paper.

In the literature, very few examples of dc voltage balancing controls operated by the DAB converters stage in the ST are proposed. In particular, in [34], the loads are supposed to be balanced and the dc voltage imbalances, caused just by mismatch of the DAB parameters, are compensated using a different PI controller for each DAB converter. For this reason, the method does not facilitate the practical implementation.

A simple and practical control to balance the dc voltages at the output of the DAB converters is proposed in [35] where the phase shift of each DAB converter is modified differently in order to achieve this purpose. However, no control tuning details are provided in [35] and the dynamics coupling among the DAB converters and the CHB converters is not taken into account. Hence, the effect of possible dc-links voltage variations of the CHB converter on the output voltage of the DAB converters is not considered in the control design.

In this work, the small signal modeling of the entire power stage leads to take into account the coupling among the CHB converter and the DAB converters dynamics. The design of the complete control system is based on the detailed small signal model of the ac–dc and dc–dc power conversion stages of the ST. The detailed model of the ST represents one of the main contributions of this work. Very few papers can be found on this topic, and in these papers, the analysis is focused just on single parts of the ST [36]–[39].

The proposed control structure of the overall system is presented in Fig. 3. The CHB converter controls the ac current and

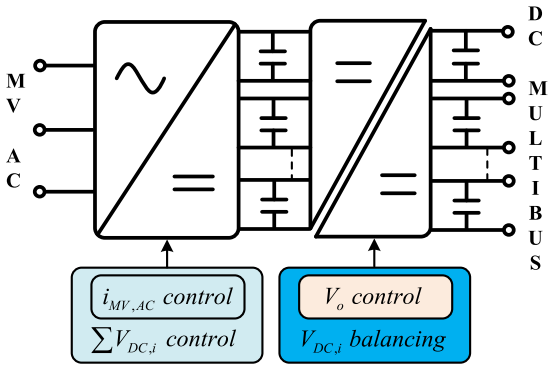

Fig. 3. ST control structure where the dc–dc stage is in charge of dc voltage balancing.

the CHB dc-links voltages, whereas the DAB converters control their dc-links output voltages, compensating the effects of voltage variations on the DAB converters output. Instability issues are avoided, because all controllers are tuned on the basis of the theoretical model of the ST and high dynamic performances can be achieved. The results are compared with the performances provided in case the dc voltage balancing is performed by the CHB converter.

The DAB converters are characterized by higher switching frequencies than the CHB converter due to the presence of a medium frequency transformer. In case of the CHB converter, such switching frequencies cannot be used in order to achieve an acceptable efficiency [40]. This peculiarity is exploited in order to improve the dynamic performance of the proposed voltage balancing control.

It represents a significant improvement since larger control bandwidth involves plug-and-play feature to the overall system, which can be able to identify and rapidly respond to changes due to dc sources insertion or disconnections, loads variations, etc.

The rest of the paper is organized as follows. In Section II, the small signal model of the first and second stage of the ST is presented, and in Section III, the proposed control scheme is described. The simulation and experimental results are discussed in Section IV. Finally, the conclusion is given in Section V.

II. Model of the Smart Transformer

The considered case study is shown in Fig. 2. An average model of the ST is shown in Fig. 4. In this model, the CHB converter is represented as the sum of *N* voltage sources connected to the main ac grid voltage *e* through an inductive filter L_g.

The output voltage $v_{AB,i}$ of each CHB power cell can be defined as

$$v_{AB,i} = m_i V_{\text{dc},i} \quad \text{with} \quad i = 1, 2, \ldots, N \tag{1}$$

where $V_{\text{dc},i}$ is the corresponding dc-link voltage and m_i is the corresponding modulating signal.

The dc current of the *i*th CHB power cell is indicated as $i_{\text{dc},i}$ and it can be defined as

$$i_{\text{dc},i} = m_i i_g \quad \text{with} \quad i = 1, 2, \ldots, N. \tag{2}$$

The DAB converters are represented both in input and in output as current sources, denoting the input current as $I_{\text{DAB},i}$ and the output current as $I_{o,i}$.

The DAB converter average model can be analytically derived studying the behavior of the current that flows through the transformer leakage inductance L_k. The input and output average currents can be evaluated, as described in [41]. Due to the symmetry of the circuit, the output and input currents over half a cycle of each DAB converter are described with the following equations:

$$I_{\text{DAB},i} = \frac{V_o T_{\text{DAB}} \varphi_i \left(1 - \varphi_i\right)}{2 L_{k,i} n} \quad \text{with} \quad i = 1, 2, \ldots, N \tag{3}$$

$$I_{o,i} = \frac{V_{\text{dc},i} T_{\text{DAB}} \varphi_i \left(1 - \varphi_i\right)}{2 L_{k,i} n} \quad \text{with} \quad i = 1, 2, \ldots, N \tag{4}$$

where *n* is the DAB transformer turn ratio, T_{DAB} represents the DAB switching period, φ(–0.5 < φ < 0.5) is the phase-shift angle (expressed in p.u. with respect to π) between the voltage at the primary and secondary side of the DAB transformer, and V_o is the DAB output voltage.

A. Model of the CHB Converter

Starting from the average model of the CHB converter defined in (1) and (2), the following equations can be derived describing the CHB converter with unitary power factor operation

$$L_g \frac{dI_g(t)}{dt} = \sum_{i=1}^{N} \left(M_i(t) V_{\text{dc},i}(t)\right) - E(t) \tag{5}$$

$$C_i \frac{dV_{\text{dc},i}(t)}{dt} = \frac{1}{2} M_i(t) I_g(t) - I_{\text{DAB},i}(t), \quad i = 1, .., N \tag{6}$$

where *E* is the amplitude of the grid voltage vector, I_g is the amplitude of the grid current vector, and *M* is the amplitude of the modulating signal vector. With a perfectly balanced load, therefore with similar voltages, each cell is driven with the same modulating signal

$$L_g \frac{dI_g(t)}{dt} = N \left(M(t) V_{\text{dc},i}(t)\right) - E(t) \tag{7}$$

$$C_i \frac{dV_{\text{dc},i}(t)}{dt} = \frac{1}{2} M(t) I_g(t) - I_{\text{DAB},i}(t), \quad i = 1, .., N. \tag{8}$$

In (7) and (8), the terms $M(t)V_{\text{dc},i}(t)$ and $M(t)I_g(t)$ are nonlinear. The small signal linearization around the equilibrium point at the rated conditions is necessary in order to derive a linear model of the CHB in the Laplace domain.

Neglecting the second-order signal perturbations, the small signal linearization of (7) and (8) leads to

$$L_g \frac{d\tilde{I}_g}{dt} = N \left(\tilde{M}\bar{V}_{\text{dc},i} + \bar{M}\tilde{V}_{\text{dc},i}\right) \tag{9}$$

$$2C_i \frac{d\tilde{V}_{\text{dc},i}}{dt} = \tilde{M}\bar{I}_g + \bar{M}\tilde{I}_g - 2\tilde{I}_{\text{DAB},i} \tag{10}$$

where $\tilde{(\cdot)}$ denotes the small perturbation and $\bar{(\cdot)}$ denotes the steady-state value. These two linear equations can be expressed

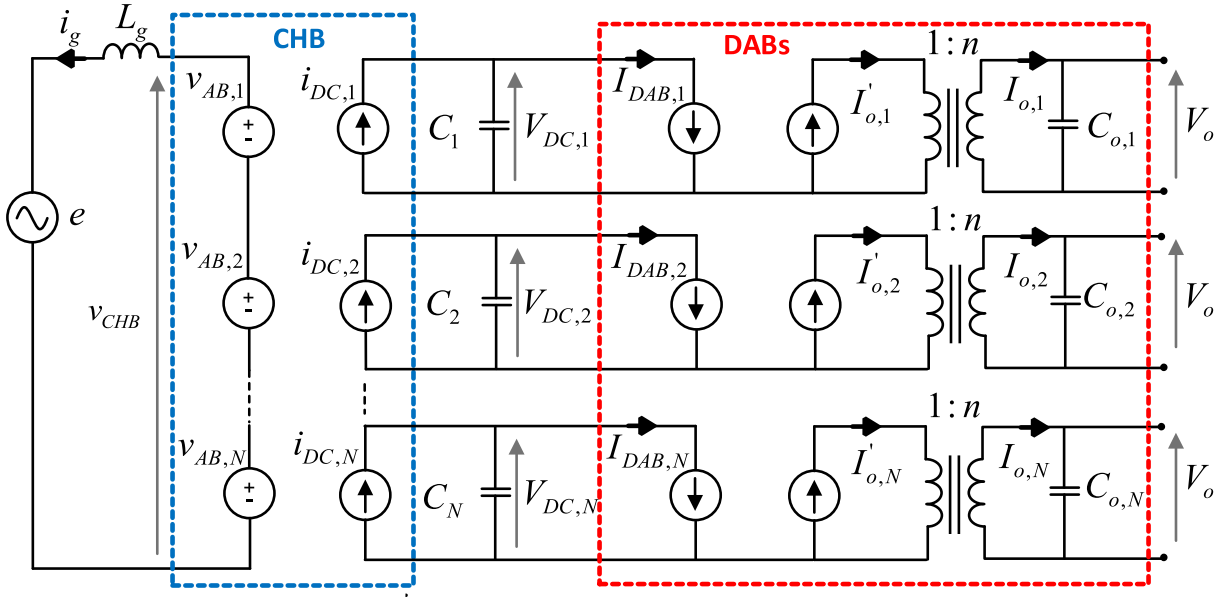

Fig. 4. CHB and DAB converters average model.

in the Laplace domain, resulting in

$$\tilde{I}_g(s) = \frac{N\bar{V}_{\mathrm{dc},i}\tilde{M}(s) + N\bar{M}\tilde{V}_{\mathrm{dc},i}(s)}{L_g s} \tag{11}$$

$$\tilde{V}_{\mathrm{dc},i}(s) = \frac{\tilde{M}(s)\bar{I}_g + \bar{M}\tilde{I}_g(s) - 2\tilde{I}_{\mathrm{DAB},i}(s)}{2C_i s}. \tag{12}$$

From (11), the small signal modulation signal $\tilde{M}$ is derived as follows:

$$\tilde{M}(s) = \frac{L_g\tilde{I}_g(s)s - N\bar{M}\tilde{V}_{\mathrm{dc},i}(s)}{N\bar{V}_{\mathrm{dc},i}}. \tag{13}$$

By substituting (13) into (12), the transfer function between each dc-link voltage and the correspondent ac current and input current of the DAB results in

$$\tilde{V}_{\mathrm{dc},i}(s) = \frac{\overline{V}_{\mathrm{dc},i}(T_z s+1)}{\overline{I}_g\,(T_p s+1)}\tilde{I}_g\,(s) - \frac{2\overline{V}_{\mathrm{dc},i}}{\overline{I}_g\,\overline{M}\,(T_p s+1)}\tilde{I}_{\mathrm{DAB},i}\,(s) \tag{14}$$

where T_z and T_p are defined as follows:

$$T_z = \frac{\bar{I}_g L_g}{N\bar{V}_{\mathrm{dc},i}\bar{M}}, \quad T_p = \frac{2\bar{V}_{\mathrm{dc},i}C_i}{\bar{I}_g\bar{M}}. \tag{15}$$

Equation (14) indicates that the voltage variation on the dc link of each H-bridge depends both on the grid current $\tilde{I}_g$ and dc current $\tilde{I}_{\mathrm{DAB},i}$ variations. In the model, $\tilde{I}_{\mathrm{DAB},i}$ is considered as a disturbance to be rejected by the voltage control loop. The small signal model of the CHB converter is depicted in Fig. 5.

B. Model of the DAB Converters

The average model of the DAB, as presented in (3) and (4), contains nonlinearity in the actuating term $\varphi_i(1-\varphi_i)$. Furthermore, this term is multiplied in (3) with the controlled output voltage V_o, and in (4), it is multiplied with the input voltage $V_{\mathrm{dc},i}$.

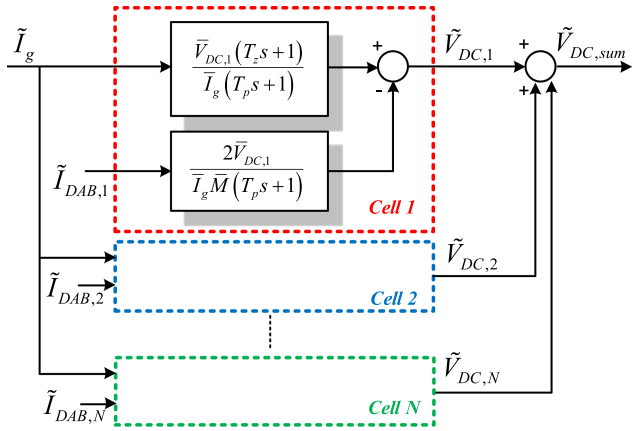

Fig. 5. Small signal model of the $2N+1$ level CHB converter.

In order to control the output voltage with a linear controller, it becomes necessary to derive a linear model of the DAB converter around a stable steady-state point. Considering (3) and (4) and a perturbation around their steady-state points, it results

$$\tilde{I}_{\mathrm{DAB},i} = \frac{T_{\mathrm{DAB}}}{2L_{k,i}n}\left[\tilde{\varphi}_i\left(1-2\bar{\Phi}_i\right)\bar{V}_o + \tilde{V}_o\left(1-\bar{\Phi}_i\right)\bar{\Phi}_i\right] \tag{16}$$

$$\tilde{I}_{o,i} = \frac{T_{\mathrm{DAB}}}{2L_{k,i}n}\left[\tilde{\varphi}_i\left(1-2\bar{\Phi}_i\right)\bar{V}_{\mathrm{dc},i} + \tilde{V}_{\mathrm{dc},i}\left(1-\bar{\Phi}_i\right)\bar{\Phi}_i\right]. \tag{17}$$

It is assumed that all the DAB converters have the same parameters. For the modeling, all the DAB converters are assumed to provide the same output voltage V_o, which is the dc voltage level chosen for the power distribution system in the smart grid. Considering that some of the outputs of the dc multibus can be connected in parallel on the basis of the configuration of the dc smart grid, the small signal model of the

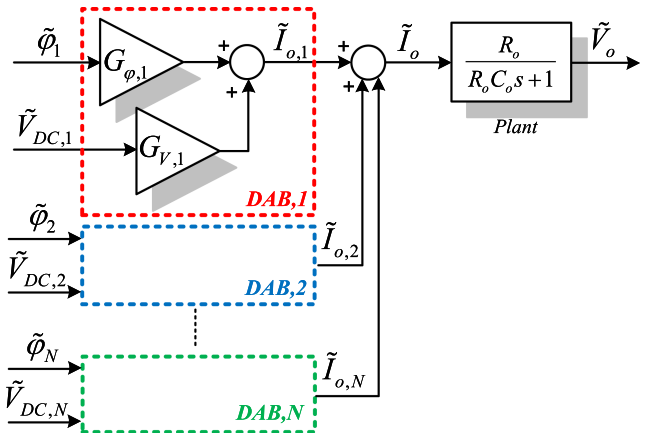

Fig. 6. Small signal model of the dc–dc power conversion stage.

overall dc–dc power conversion stage is derived assuming that the DAB converters outputs are parallel connected and supply a resistive load denoted as R_o

$$\tilde{I}_o = \sum_{i=1}^{N} \tilde{I}_{o,i}, \quad \tilde{V}_o(s) = \frac{R_o}{(R_o N C_{o,i} s + 1)} \tilde{I}_o. \tag{18}$$

Hence, substituting (17) into (18), it results in

$$\tilde{V}_o(s) = \frac{R_o}{(R_o C_o s + 1)} \sum_{i=1}^{N} \left\{ \frac{T_{\text{DAB}}}{2L_{k,i} n} \left[\tilde{\varphi}_i \left(1 - 2\bar{\Phi}_i\right) \bar{V}_{\text{dc},i} + \tilde{V}_{\text{dc},i} \left(1 - \bar{\Phi}_i\right) \bar{\Phi}_i \right\} \right. \tag{19}$$

It is possible to define two constant gains as

$$G_{\varphi,i} = \frac{T_{\text{DAB}}}{2L_{k,i} n} \left(1 - 2\bar{\Phi}_i\right) \bar{V}_{\text{dc},i}$$

$$G_{V,i} = \frac{T_{\text{DAB}}}{2L_{k,i} n} \left(1 - \bar{\Phi}_i\right) \bar{\Phi}_i. \tag{20}$$

Hence, the final expression of the output voltage loop is

$$\tilde{V}_o(s) = \left(\frac{R_o}{R_o C_o s + 1}\right) \sum_{i=1}^{N} \left[G_{\varphi,i} \tilde{\varphi}_i + G_{V,i} \tilde{V}_{\text{dc},i} \right]. \tag{21}$$

In such control system, $\tilde{V}_o$ is the controlled variable, $\tilde{\varphi}_i$ is the input, $\tilde{V}_{\text{dc},i}$ is considered as an external disturbance, and $R_o C_o$ is the plant time constant. The small signal model of the dc–dc power conversion stage is presented in Fig. 6.

III. Proposed Control System

With regard to the case study presented in Fig. 2 and to the control features shown in Fig. 3, the overall control system of the first two stages of the ST can be designed as proposed in the following.

A. CHB Converter Control System

The basic control functions of the CHB converter are the dc voltage control and the ac current control. The outer dc voltage control loop provides the reference to an internal current control loop, as shown in Fig. 7. Details about the CHB converter modulation can be found in [4]. Processing a single-phase sinusoidal current, the P + Resonant (PR) controller is a good choice for the inner current loop as already demonstrated in [42].

The proportional and resonant gain of the PR controller can be tuned to achieve optimal damping (damping factor $\zeta = 0.707$) and short settling times corresponding to an overshoot around 5% in the step response [43]. In this hypothesis, a second-order transfer function can be used as a good approximation of the current loop transfer function based on a PR controller:

$$H_{I_g}(s) = \frac{I_g}{I_g^*} \approx \frac{\frac{2}{(3T_s)^2}}{s^2 + \frac{2}{3T_s} s + \frac{2}{(3T_s)^2}}. \tag{22}$$

The outer loop is based on a PI controller and the parameters of the PI voltage controller can be tuned in order to decouple the internal current loop and the external voltage loop dynamics. The open-loop transfer function of the overall dc voltage control loop is

$$G_{V_{\text{dc}}}(s) = \frac{K_p (T_i s + 1)}{T_i s} H_{I_g}(s) \left(\frac{N \bar{V}_{\text{dc},i} (T_z s + 1)}{\bar{I}_g (T_p s + 1)} \right) \tag{23}$$

where K_p is the proportional gain and T_i is the integral time constant. The design of the voltage control loop is made in order to obtain a dynamics, which is ten times slower than the closed-loop current dynamics at least.

As first step, the PI integrator time constant T_i has been chosen equal to the plant time constant T_p. Considering a perfect pole-zero cancellation, the voltage open-loop transfer function in the Laplace domain is

$$G_{V_{\text{dc}}}(s) = \left(\frac{K_p \bar{M} N}{2C_i} \right) \frac{(T_z s + 1)}{s} H_{I_g}(s). \tag{24}$$

If the current control loop is adjusted to be optimally damped, a first-order approximation can be useful when calculating the bandwidth of the system and when designing the voltage loop with a bandwidth smaller than the one of the current loop [43]

$$H_{I_g}(s) \approx \frac{1}{(3T_s s + 1)}, \quad f_{\text{BW\_CC}} = \frac{1}{6\pi T_s}. \tag{25}$$

Substituting the first-order current loop approximation of (25) into (24), a new simplified open-loop transfer function is derived

$$G_{V_{\text{dc}}}(s) = \frac{k (T_z s + 1)}{s (3T_s s + 1)} \quad \text{with} \quad k = \frac{K_p \bar{M} N}{2C_i}. \tag{26}$$

Starting from (26), the closed-loop transfer function of the voltage controller is

$$H_{V_{\text{dc}}}(s) = \frac{k (T_z s + 1)}{3T_s s^2 + (k T_z + 1) s + k}. \tag{27}$$

This equation shows the dependence of the closed-loop transfer function on the value of K_p, which is the only tunable parameter to guarantee the bandwidth specifications.

The entire cascaded control system based on the small signal model of the CHB converter is presented in Fig. 7.

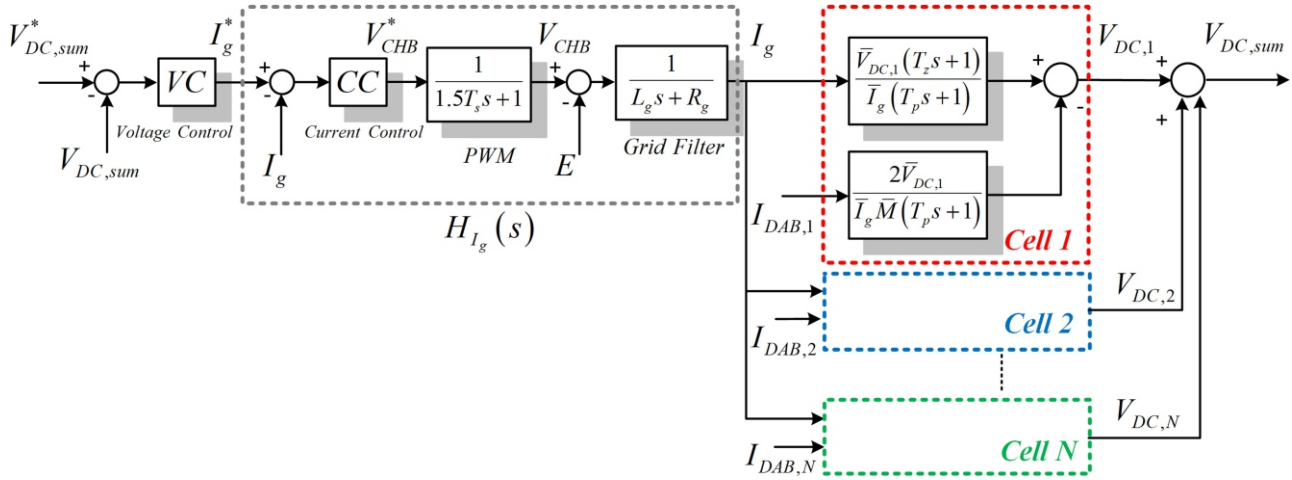

Fig. 7. Control scheme of the CHB converter.

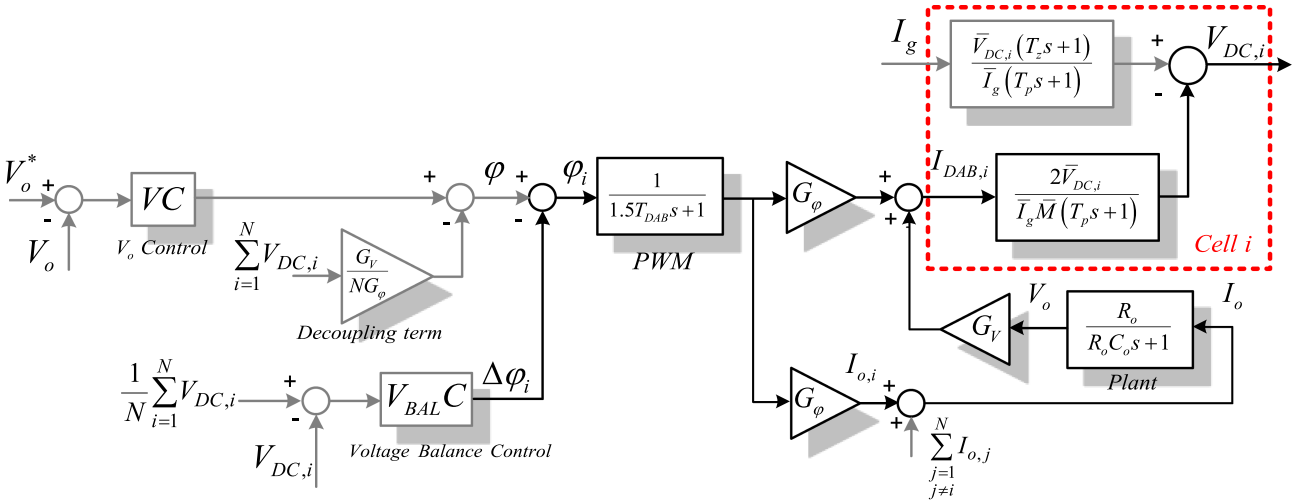

Fig. 8. Control scheme of the ST dc–dc power conversion stage.

B. DAB Converters Control System

The main task of the DAB converters control system is the regulation of the common output voltage V_o to its reference value. The control scheme of the DAB converter is shown in Fig. 8. Starting from the equation of the DAB converters output voltage

$$\tilde{V}_o(s) = \left(\frac{R_o}{R_o C_o s+1}\right)\left(NG_\varphi \tilde{\varphi} + G_V \sum_{i=1}^{N} \tilde{V}_{\mathrm{dc},i}\right) \quad (28)$$

a control law can be defined, which considers φ as the control variable and $V_{\mathrm{dc},i}$ as a measurable disturbance. The effect of the input voltage variations $\tilde{V}_{\mathrm{dc},i}$ of the DAB converters on the output voltage V_o can be compensated introducing a feed-forward action whose effect is added up with the feedback control. Just in this hypothesis, the DAB converters control can be decoupled by what occurs in the CHB converter. Hence, the control law results in

$$\tilde{\varphi} = K_{p_o}\left(1+\frac{1}{T_{i_o} s}\right)\left(\tilde{V}^*_o - \tilde{V}_o\right) - \frac{G_V}{NG_\varphi}\sum_{i=1}^{N} \tilde{V}_{\mathrm{dc},i}. \quad (29)$$

The final open-loop transfer function is the following:

$$G_{Vo}(s) = NG_\varphi K_{p_o}\left(\frac{T_{i_o} s+1}{T_{i_o} s}\right)\left(\frac{R_o}{R_o C_o s+1}\right) \quad (30)$$

where K_{po} and T_{io} are, respectively, the proportional gain and the integral time constant. Choosing T_{io} equal to $R_o C_o$ (pole-zero cancellation), the closed-loop transfer function $H_{Vo}(s)$ is derived as follows:

$$H_{Vo}(s) = \frac{1}{\left(1+\frac{s}{K_{\mathrm{DAB}} K_{p_o}}\right)} \quad \text{with} \quad K_{\mathrm{DAB}} = \frac{NG_\varphi}{C_o}. \quad (31)$$

It results in a first-order system, with reference tracking and disturbance rejection capability depending on the value of the proportional gain.

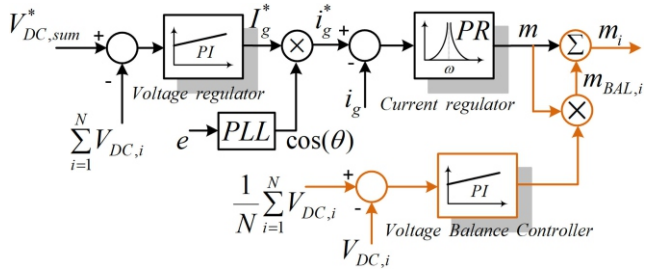

Fig. 9. CHB control scheme in case the CHB is balancing the voltages.

C. DC Voltage Balancing Control

The voltage balancing control is based on a PI controller for each dc link. The phase shift angle for each DAB converter is corrected by subtracting the contribution of the voltage balancing controller $\Delta\varphi_i$. This is shown in Fig. 8. Hence, in case of an ST with *N* power cells, the phase shift for each DAB converter can be calculated as

$$\tilde{\varphi}_i = \varphi - K_{p\mathrm{BAL},i}\left(1+\frac{1}{T_{\mathrm{BAL},i}s}\right)\left(\frac{1}{N}\sum_{i=1}^{N}\tilde{V}_{\mathrm{dc},i}-\tilde{V}_{\mathrm{dc},i}\right) \tag{32}$$

where $K_{p\mathrm{BAL},i}$ is the voltage balancing proportional gain related to the *i*th dc link. $T_{\mathrm{BAL},i}$ is the voltage balancing controller integral time constant, which is tuned to guarantee zero steady-state error.

Considering also the acquisition and the pulsewidth modulation (PWM) time delay, the open-loop transfer function of the voltage balancing control between the *i*th dc-link voltage and $\Delta\varphi_i$ can be easily derived in Fig. 8. It results in

$$V_{\mathrm{dc},i}(s) = \frac{2G_\varphi}{3T_{\mathrm{DAB}}C_i} \times \frac{1}{\left(s+\frac{1}{T_p}\right)\left(s+\frac{2}{3T_{\mathrm{DAB}}}\right)}\frac{\left(s+\frac{1+G_V R_o}{R_o C_o}\right)}{\left(s+\frac{1}{R_o C_o}\right)}\Delta\varphi_i. \tag{33}$$

Choosing $T_{\mathrm{BAL},i} = T_p$ and thereby cancelling the slowest pole, the new open-loop transfer function is

$$G_{\mathrm{BAL},i}(s) \approx \frac{K_{p\mathrm{BAL},i}G_\varphi}{C_i s\left(1.5T_{\mathrm{DAB}}s+1\right)}. \tag{34}$$

Equation (34) shows the relationship between the parameters of the dc voltage balancing controller and the theoretical model of the ST.

For a comparison of the control schemes, the voltage balancing control performed by the CHB is shown in Fig. 9.

In Fig. 9, $V_{\mathrm{dc},i}$ is the dc voltage measured at the *i*th dc link of the CHB converter, i^*_g is the current reference, and $m_{\mathrm{BAL},i}$ represents the contribution to the modulating signal of the *i*th H-bridge in order to balance the dc voltage.

The modulating signal for the *i*th H-bridge is defined as

$$m_i = m\left[1+K_{p\mathrm{BAL},i}\left(1+\frac{1}{T_{\mathrm{BAL},i}s}\right)\left(\frac{1}{N}\sum_{i=1}^{N}V_{\mathrm{dc},i}-V_{\mathrm{dc},i}\right)\right] \tag{35}$$

where $K_{p\mathrm{BAL},i}$ and $T_{\mathrm{BAL},i}$ are, respectively, the proportional gain and the integral time constant of the *i*th CHB cell voltage balancing controller. By varying the parameters, it is possible to regulate the control action.

The open-loop transfer function of the voltage balancing loop $G_{\mathrm{BAL},i}(s)$ can be derived in Fig. 10, where the PI controller transfer function, the model of the PWM time delay, the inductive grid filter, and the *i*th dc-link model are taken into account

$$G_{\mathrm{BAL},i}(s) = \frac{M}{2}K_{p\mathrm{BAL},i}\left(1+\frac{1}{T_{\mathrm{BAL},i}s}\right)\left(\frac{1}{1.5T_s s+1}\right) \times \left(\frac{1}{L_g s+R_g}\right)\left(\frac{R_i}{R_i C_i s+1}\right). \tag{36}$$

IV. Simulation and Experimental Results

With the aim to validate the effectiveness of the proposed control structure and the theoretical models of the overall system, an experimental setup related to a small-scale ST has been built and it is shown in Fig. 11. Due to the experimental setup constraints, the first two stages of the ST consist of a five-level CHB converter connected to the distribution grid and feeding power to two DAB converters. The DAB power modules are parallel connected in output and they supply a resistive load. The H-bridges in the CHB converter and the DAB converters are based on DP25H1200T101616IGBT Danfoss module and the system is controlled with a dSPACE SCALEXIO platform based on three DS2655FPGA boards; each board is programmed with an FPGA Xilinx blockset toolbox. The power stage parameters are summarized in Table I.

A. CHB and DAB Converters Model and Control Validation

For the validation of the CHB model, the responses of the system to a reference voltage step ($\Delta V^*_{\mathrm{dc}} = 10$ V) are compared. This is shown in Fig. 12, where the step is applied at $t = 1$ s and the small signal model response, the average model response, and experimental results are compared. As can be seen, the voltage provided by the real system tracks the response provided by the models.

Similarly, the responses of the DAB converter in case of a reference voltage step ($\Delta V^*_o = 1$ V) have been compared by considering the output voltage provided experimentally and the results provided by the average and the small signal model in simulation. As in the previous case, the analytical results match well with the experimental results (see Fig. 13). Finally, the effects of power variations on the dc-link voltages are analyzed: at $t = 0.5$ s, the power processed by the first DAB converter is increased and the power processed by the second DAB converter is reduced by maintaining constant the overall output power. It can be observed that the power step implies a transient voltage variation for each dc link and the small signal model response tracks the average model without significant deviations (see Fig. 14).

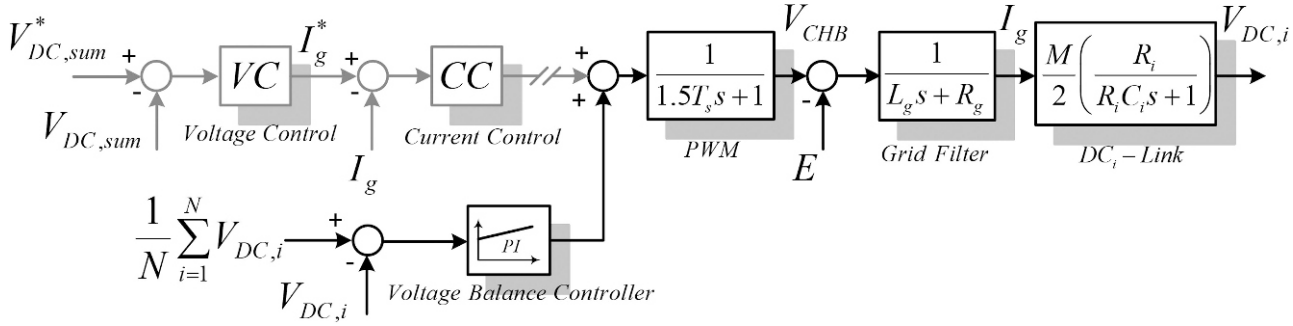

Fig. 10. Detailed voltage control scheme in case of voltage balancing in the CHB stage.

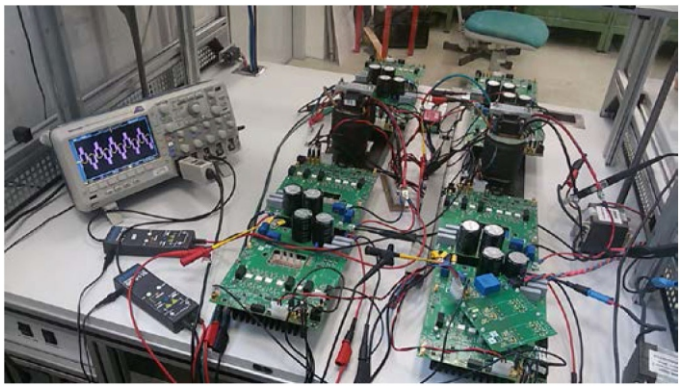

Fig. 11. Small-scale ST experimental setup: ac–dc and dc–dc power conversion stage.

TABLE I
POWER STAGE PARAMETERS

Symbol	Description	Value
e	Grid Voltage (RMS)	230 V, 50 Hz
L_g	Filter Inductance (MV side)	3.8 mH
$V_{DC,1}$=$V_{DC,2}$	DC-Link voltage MV side	250 V
V_o	DC-link voltage LV side	250 V
C_1=C_2	MV capacitance	930 μF
C_o	LV capacitance	920 μF
R_o	Load resistance	32 Ω
$L_{k,1}$= $L_{k,2}$	Leakage inductance MFT	63 μH
n	MFT turn ratio	1
$f_{sw,CHB}$	CHB switching frequency	3 kHz
$f_{sw,DAB}$	DAB switching frequency	12 kHz
P_n	ST nominal power	2 kW

B. Performance Comparison of the Balancing Solutions

Finally, a comparison between the performances of the proposed voltage balancing technique and the voltage balancing performed by the CHB is provided. Considering the open-loop transfer functions of the balancing loops, as reported in (34) for the DAB converters and in (36) for the CHB converter, the crossover frequency provides information about the bandwidth and the dynamics. For the DAB converters stage, the bandwidth has been designed in order to obtain a voltage balancing control as fast as the current control loop in the CHB stage

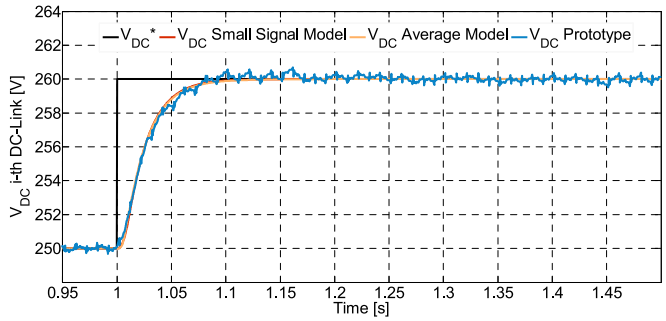

Fig. 12. CHB converter: response of the system in case of a reference voltage step $\Delta V^*_{\rm dc} = 10\,{\rm V}$ ($T_{\rm settling} = 100\,{\rm ms}$).

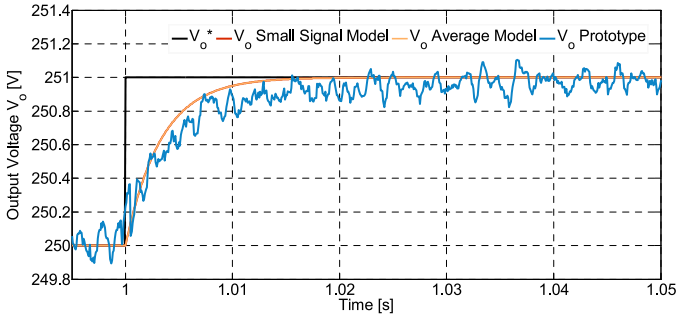

Fig. 13. DAB converters: response of the system in case of a reference voltage step $\Delta V^*_o = 1\,{\rm V}$ ($T_{\rm settling} = 10\,{\rm ms}$).

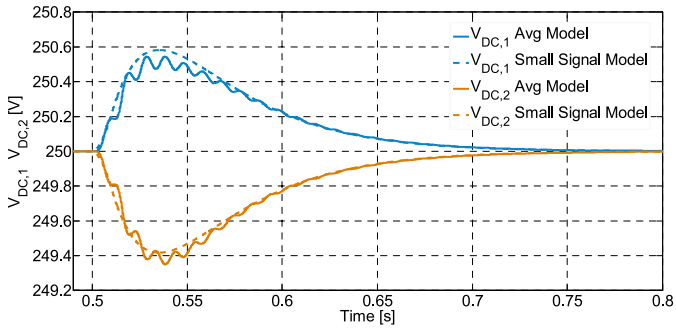

Fig. 14. DAB converters dc-link voltages $V_{dc,1}$ and $V_{dc,2}$ in case of variations of the power processed by each cell.

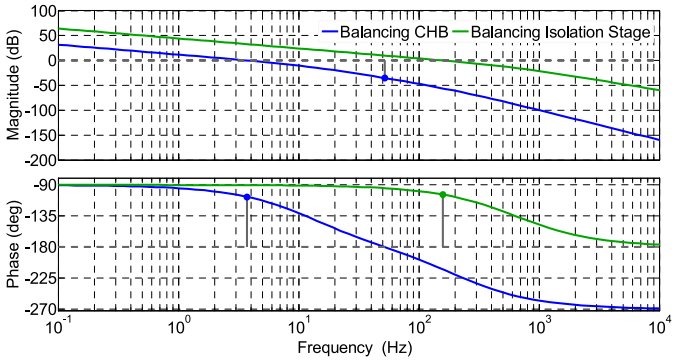

Fig. 15. Comparison of the bandwidth for voltage balancing in the CHB stage and in the DAB converters stage.

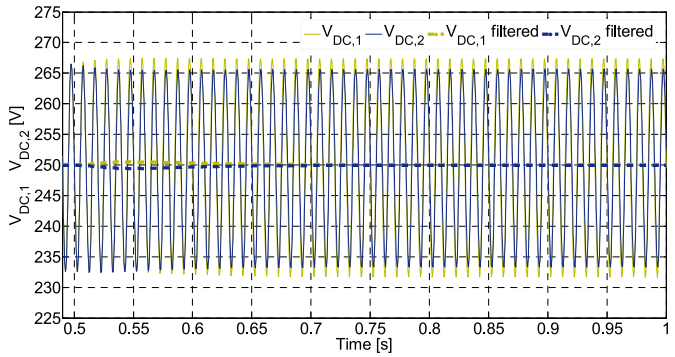

Fig. 16. DAB converters voltage balancing control: dc-link voltages in case of a power step for DAB_1 and DAB_2 (simulation results).

($f_{\text{BW\_CC}} = 160\,\text{Hz}$). As a result, the phase margin is around 75°, which is a good compromise between robustness and dynamics.

For a fair comparison of the two balancing controllers, the bandwidth of the balancing control loop in the CHB stage has been chosen in order to guarantee the same robustness (same PM). The result, in this case, is a low bandwidth (4 Hz). If the target is to reach a bandwidth of 160 Hz, the balancing method in the CHB stage is unstable. This demonstrates the better performance of the proposed balancing method in comparison to the classical approach.

For the demonstration, the frequency responses of the two balancing controllers are shown in Fig. 15. A significant difference in the bandwidth ($\text{BW}_{\text{CHB}} = 4\,\text{Hz}$, $\text{BW}_{\text{DAB}} = 160\,\text{Hz}$) of the two control systems and consequently in the disturbance rejection capability is observed.

The voltage balancing control operated by the dc–dc power conversion stage of the ST exhibits superior performances than the voltage balance control operated by the ac–dc converter of the ST. This is because of the higher switching frequency in the dc–dc power conversion stage than in the CHB.

The different dynamic performances can be observed also in Figs. 16 and 17, where the dc-link voltages of the five-level CHB converter are shown moving from a power balance to a power unbalance condition. Starting from $P_{DAB,1} = P_{DAB,2} = 1\,\text{kW}$, the DAB converters power reference is changed in $P_{DAB,1} = 1.5\,\text{kW}$ and $P_{DAB,2} = 0.5\,\text{kW}$. As expected from Fig. 15, the

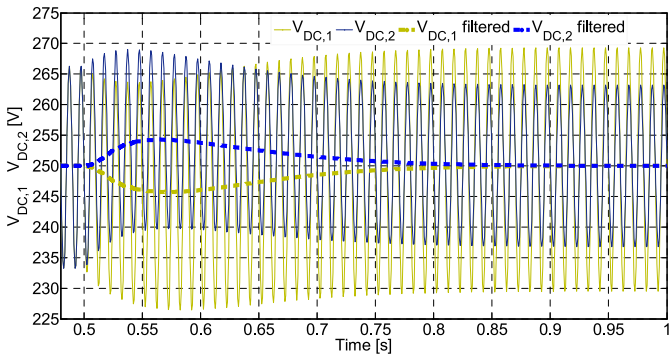

Fig. 17. CHB voltage balancing control: dc-link voltages in case of a power step for the two H-bridges (simulation results).

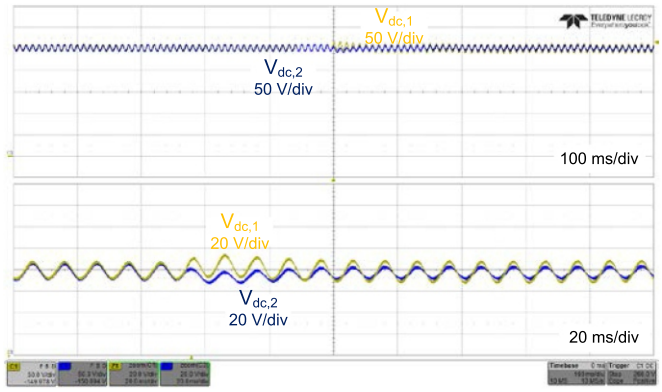

Fig. 18. DAB converters voltage balancing control: dc-link voltages in case of a power step for $P_{DAB,1}$ and $P_{DAB,2}$ (experimental results).

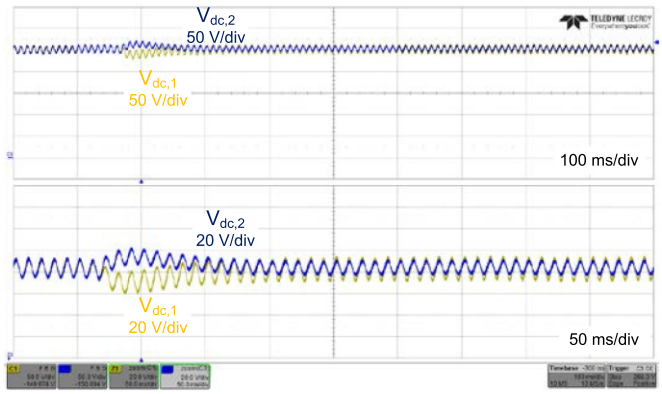

Fig. 19. CHB voltage balancing control: dc-link voltages in case of a power step for the two power modules (experimental results).

response provided by the proposed control system is faster than the response of the voltage balancing performed by the CHB converter.

The simulation results are validated experimentally with experiments similar to those performed previously. Results are shown in Figs. 18 and 19.

As expected from the simulation results, the transient behavior duration related to the balancing control in the dc–dc stage is shorter than the transient behavior duration related to

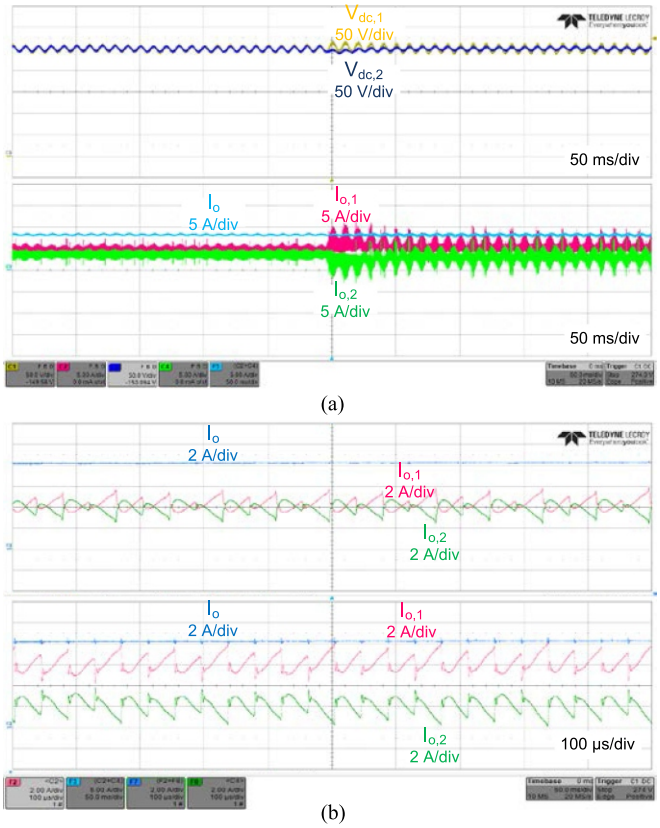

Fig. 20. DAB voltage balancing control. (a) Output currents $I_{o,1}$, $I_{o,2}$, and I_o during the variation. (b) Zoom of the same currents.

the balancing control in the CHB stage and also the transient peak voltage is lower. It provides information about high rejection to external disturbances and it suggests using the voltage balancing method in the isolation stage rather than in the medium voltage stage. Remarkably, the experimental results fit the simulation results shown in Figs. 16 and 17.

Finally, Fig. 20(a) shows the output currents of the two DAB converters before and after the change in the power references. Before the change in the reference, the output currents of the DAB converters have the same mean value and their ripples cancel out each other. The overall output current is $I_o = 8$ A. After the power variation, the output currents of the DAB converters are $I_{o,1} = 6$ A and $I_{o,2} = 2$ A. Because of the unequal power sharing between the DAB converters, the currents exhibit higher harmonic distortion [see Fig. 20(b)]. The increased distortion is the drawback of the presence of a circulating current path when the DAB converters work with different phase shifts, sharing a different power to the load.

V. Conclusion

One of the main issues in a modular ST is the dc voltage balancing among the power cells. In case of a three-stage architecture based on a CHB converter for the ac–dc power conversion stage and DAB converters for the dc–dc power conversion stage, the CHB converter is commonly in charge of the voltage balancing. However, looking at the overall ST system, it can be advantageous that the dc–dc power conversion stage is in charge of the dc voltage balancing, because in dc smart grids the power flow is commonly not balanced. With the proposed control technique, the dynamic performance of the voltage balancing is improved, ensuring a larger bandwidth than the traditional control method. It is due to the higher switching frequency of the dc–dc power conversion stage than the switching frequency of the ac–dc power conversion stage.

References

[1] G. J. Kish, "On the emerging class of non-isolated modular multilevel dc-dc converters for dc and hybrid ac-dc systems," *IEEE Trans. Smart Grid*, to be published, doi: 10.1109/TSG.2017.2777473.

[2] S. Grillo, V. Musolino, L. Piegari, E. Tironi, and C. Tornelli, "DC islands in ac smart grids," *IEEE Trans. Power Electron.*, vol. 29, no. 1, pp. 89–98, Jan. 2014.

[3] B. Wang, M. Sechilariu, and F. Locment, "Intelligent dc microgrid with smart grid communications: Control strategy consideration and design," *IEEE Trans. Smart Grid*, vol. 3, no. 4, pp. 2148–2156, Dec. 2012.

[4] R. A. Mastromauro, S. Pugliese, D. Ricchiuto, S. Stasi, and M. Liserre, "DC multibus based on a single-star bridge cells modular multilevel cascade converter for dc smart grids," in *Proc. Int. Conf. Clean Electr. Power*, Taormina, Italy, 2015, pp. 55–60.

[5] Z. Jin, G. Sulligoi, R. Cuzner, L. Meng, J. C. Vasquez, and J. M. Guerrero, "Next-generation shipboard dc power system: Introduction smart grid and dc microgrid technologies into maritime electrical networks," *IEEE Electrif. Mag.*, vol. 4, no. 2, pp. 45–57, Jun. 2016.

[6] F. D. Kanellos, G. J. Tsekouras, and J. Prousalidis, "Onboard dc grid employing smart grid technology: Challenges, state of the art and future prospects," *IET Electr. Syst. Transp.*, vol. 5, no. 1, pp. 1–11, 2015.

[7] T. Morstyn, B. Hredzak, G. D. Demetriades, and V. G. Agelidis, "Unified distributed control for dc microgrid operating modes," *IEEE Trans. Power Syst.*, vol. 31, no. 1, pp. 802–812, Jan. 2016.

[8] Z. X. Zou, G. De Carne, G. Buticchi, and M. Liserre, "Smart transformer-fed variable frequency distribution grid," *IEEE Trans. Ind. Electron.*, vol. 65, no. 1, pp. 749–759, Jan. 2018.

[9] X. Gao, F. Sossan, K. Christakou, M. Paolone, and M. Liserre, "Concurrent voltage control and dispatch of active distribution networks by means of smart transformer and storage," *IEEE Trans. Ind. Electron.*, vol. 65, no. 8, pp. 6657–6666, Aug. 2018.

[10] T. L. Vandoorn, J. D. M. De Kooning, B. Meersman, J. M. Guerrero, and L. Vandevelde, "Voltage-based control of a smart transformer in a microgrid," *IEEE Trans. Ind. Electron.*, vol. 60, no. 4, pp. 1291–1305, Apr. 2013.

[11] R. Zhu, G. De Carne, F. Deng, and M. Liserre, "Integration of large photovoltaic and wind system by means of smart transformer," *IEEE Trans. Ind. Electron.*, vol. 64, no. 11, pp. 8928–8938, Nov. 2017.

[12] H. Chen and D. Divan, "Design of a 10 kVA soft-switching solid state transformer (S4T)," *IEEE Trans. Power Electron.*, vol. 33, no. 7, pp. 5724–5738, Jul. 2018.

[13] B. Zhao, Q. Song, J. Li, and W. Liu, "A modular multilevel dc-link front-to-front dc solid-state transformer based on high-frequency dual active phase shift for HVDC grid integration," *IEEE Trans. Ind. Electron.*, vol. 64, no. 11, pp. 8919–8927, Nov. 2017.

[14] M. Andresen, L. F. Costa, G. Buticchi, and M. Liserre, "Smart transformer reliability and efficiency through modularity," in *Proc. IEEE 8th Int. Power Electron. Motion Control Conf.*, Hefei, China, 2016, pp. 3241–3248.

[15] P. Xu *et al.*, "The redundancy fault-tolerant control strategies for modular solid state transformer with dc bus," in *Proc. IEEE 3rd Int. Future Energy Electron. Conf. ECCE Asia*, Kaohsiung, Taiwan, 2017, pp. 1997–2001.

[16] L. F. Costa, G. Buticchi, and M. Liserre, "Highly efficient and reliable SiC-Based dc–dc converter for smart transformer," *IEEE Trans. Ind. Electron.*, vol. 64, no. 10, pp. 8383–8392, Oct. 2017.

[17] T. Yao, I. Leonard, R. Ayyanar, and M. Steurer, "Single-phase three-stage SST modeling using RTDS for controller hardware-in-the-loop application," in *Proc. IEEE Energy Convers. Congr. Expo.*, Montreal, QC, Canada, 2015, pp. 2302–2309.

[18] L. F. Costa, G. Buticchi, and M. Liserre, "Modular smart transformer architectures: An overview and proposal of a interphase architecture," in *Proc. IEEE 8th Int. Symp. Power Electron. Distrib. Gener. Syst.*, Florianopolis, Brazil, 2017, pp. 1–7.

[19] D. Ricchiuto, R. A. Mastromauro, M. Liserre, I. Trintis, and S. Munk-Nielsen, "Overview of multi-dc-bus solutions for dc microgrids," in *Proc. 4th IEEE Int. Symp. Power Electron. Distrib. Gener. Syst.*, Rogers, AR, USA, 2013, pp. 1–8.

[20] L. Tarisciotti, P. Zanchetta, A. Watson, S. Bifaretti, J. C. Clare, and P. W. Wheeler, "Active dc voltage balancing PWM technique for high power cascaded multilevel converters," *IEEE Trans. Ind. Electron.*, vol. 61, no. 11, pp. 6157–6167, Nov. 2014.

[21] M. Moosavi, G. Farivar, H. Iman-Eini, and S. M. Shekarabi, "A voltage balancing strategy with extended operating region for cascaded H-bridge converters," *IEEE Trans. Power Electron.*, vol. 29, no. 9, pp. 5044–5053, Sep. 2014.

[22] A. Moeini and S. Wang, "A dc link voltage balancing technique for cascaded H-bridge multilevel converters with asymmetric selective harmonic current mitigation-PWM," *IEEE Trans. Power Electron.*, to be published, doi: 10.1109/TPEL.2017.2770141.

[23] J. A. Barrena, L. Marroyo, M. Á. Rodriguez Vidal, and J. R. Torrealday Apraiz, "Individual voltage balancing strategy for PWM cascaded H-bridge converter-based STATCOM," *IEEE Trans. Ind. Electron.*, vol. 55, no. 1, pp. 21–29, Jan. 2008.

[24] H. Iman-Eini, J. L. Schanen, S. Farhangi, and J. Roudet, "A modular strategy for control and voltage balancing of cascaded H-bridge rectifiers," *IEEE Trans. Power Electron.*, vol. 23, no. 5, pp. 2428–2442, Sep. 2008.

[25] J. I. Leon, R. Portillo, S. Vazquez, J. J. Padilla, L. G. Franquelo, and J. M. Carrasco, "Simple unified approach to develop a time-domain modulation strategy for single-phase multilevel converters," *IEEE Trans. Ind. Electron.*, vol. 55, no. 9, pp. 3239–3248, Sep. 2008.

[26] X. She, A. Q. Huang, T. Zhao, and G. Wang, "Coupling effect reduction of a voltage-balancing controller in single-phase cascaded multilevel converters," *IEEE Trans. Power Electron.*, vol. 27, no. 8, pp. 3530–3543, Aug. 2012.

[27] T. Zhao, G. Wang, S. Bhattacharya, and A. Q. Huang, "Voltage and power balance control for a cascaded H-bridge converter-based solid state transformer," *IEEE Trans. Power Electron.*, vol. 28, no. 4, pp. 1523–1532, Apr. 2013.

[28] X. Wang, J. Liu, S. Ouyang, T. Xu, F. Meng, and S. Song, "Control and experiment of an H-bridge-based three-phase three-stage modular power electronic transformer," *IEEE Trans. Power Electron.*, vol. 31, no. 3, pp. 2002–2011, Mar. 2016.

[29] V. Raveendran, G. Buticchi, A. Mercante, and M. Liserre, "Comparison of voltage control methods of CHB converters for power routing in smart transformer," in *Proc. IEEE Energy Convers. Congr. Expo.*, Cincinnati, OH, USA, 2017, pp. 1652–1658.

[30] J. Shi, W. Gou, H. Yuan, T. Zhao, and A. Q. Huang, "Research on voltage and power balance control for cascaded modular solid-state transformer," *IEEE Trans. Power Electron.*, vol. 26, no. 4, pp. 1154–1166, Apr. 2011.

[31] K. Xu, C. Fu, Y. Wang, and H. Wang, "Voltage and current balance control for the ISOP converter-based power electronic transformer," in *Proc. 18th Int. Conf. Electr. Mach. Syst.*, Pattaya, Thailand, 2015, pp. 378–382.

[32] M. Andresen, V. Raveendran, G. Buticchi, and M. Liserre, "Lifetime-based power routing in parallel converters for smart transformer application," *IEEE Trans. Ind. Electron.*, vol. 65, no. 2, pp. 1675–1684, Feb. 2018.

[33] V. Raveendran, M. Andresen, M. Liserre, and G. Buticchi, "Lifetime-based power routing of smart transformer with CHB and DAB converters," in *Proc. IEEE Appl. Power Electron. Conf. Expo.*, San Antonio, TX, USA, 2018, pp. 3523–3529.

[34] Z. Zhang, H. Zhao, S. Fu, J. Shi, and X. He, "Voltage and power balance control strategy for three-phase modular cascaded solid stated transformer," in *Proc. IEEE Appl. Power Electron. Conf. Expo.*, Long Beach, CA, USA, 2016, pp. 1475–1480.

[35] H.-J. Yun, H.-S. Kim, M.-H. Ryu, J.-W. Baek, and H.-J. Kim, "A simple and practical voltage balance method for a solid-state transformer using cascaded H-bridge converters," in *Proc. IEEE 9th Int. Conf. Power Electron. ECCE Asia*, 2015, pp. 2415–2420.

[36] Y. Liu, A. Q. Huang, W. Song, S. Bhattacharya, and G. Tan, "Small-signal model-based control strategy for balancing individual dc capacitor voltages in cascade multilevel inverter-based STATCOM," *IEEE Trans. Ind. Electron.*, vol. 56, no. 6, pp. 2259–2269, Jun. 2009.

[37] M. Khazraei, V. A. K. Prabhala, R. Ahmadi, and M. Ferdowsi, "Solid-state transformer stability and control considerations," in *Proc. IEEE Appl. Power Electron. Conf. Expo.*, Fort Worth, TX, USA, 2014, pp. 2237–2244.

[38] H. Sun, J. Zhang, and C. Fu, "Control strategy for dual active bridge based dc solid state transformer," in *Proc. 20th Int. Conf. Electr. Mach. Syst.*, Sydney, N.S.W., Australia, 2017, pp. 1–6.

[39] J. A. Mueller and J. W. Kimball, "Generalized average modeling of dc subsystem in solid state transformers," in *Proc. IEEE Energy Convers. Congr. Expo.*, Cincinnati, OH, USA, 2017, pp. 1659–1666.

[40] J. E. Huber and J. W. Kolar, "Optimum number of cascaded cells for high-power medium-voltage ac–dc converters," *IEEE J. Emerging Sel. Topics Power Electron.*, vol. 5, no. 1, pp. 213–232, Mar. 2017.

[41] A. Rodríguez Alonso, J. Sebastian, D. G. Lamar, M. M. Hernando, and A. Vazquez, "An overall study of a dual active bridge for bidirectional dc/dc conversion," in *Proc. IEEE Energy Convers. Congr. Expo.*, Atlanta, GA, USA, 2010, pp. 1129–1135.

[42] R. A. Mastromauro, M. Liserre, and A. Dell'Aquila, "Study of the effects of inductor nonlinear behavior on the performance of current controllers for single-phase PV grid converters," *IEEE Trans. Ind. Electron.*, vol. 55, no. 5, pp. 2043–2052, May 2008.

[43] R. Teodorescu, M. Liserre, and P. Rodriguez, *Grid Converters for Photovoltaic and Wind Power Systems*. Hoboken, NJ, USA: Wiley, 2011.